nature chemistry

ARTICLES

PUBLISHED ONLINE: 20 APRIL 2014 | DOI: 10.1038/NCHEM.1921

Fatty acid membrane assembly on coacervate microdroplets as a step towards a hybrid protocell model

T-Y. Dora Tang[1], C. Rohaida Che Hak[1], Alexander J. Thompson[2], Marina K. Kuimova[2], D. S. Williams[1], Adam W. Perriman[1] and Stephen Mann[1]*

Mechanisms of prebiotic compartmentalization are central to providing insights into how protocellular systems emerged on the early Earth. Protocell models are based predominantly on the membrane self-assembly of fatty-acid vesicles, although membrane-free scenarios that involve liquid–liquid microphase separation (coacervation) have also been considered. Here we integrate these alternative models of prebiotic compartmentalization and develop a hybrid protocell model based on the spontaneous self-assembly of a continuous fatty-acid membrane at the surface of preformed coacervate microdroplets prepared from cationic peptides/polyelectrolytes and adenosine triphosphate or oligo/polyribonucleotides. We show that the coacervate-supported membrane is multilamellar, and mediates the selective uptake or exclusion of small and large molecules. The coacervate interior can be disassembled without loss of membrane integrity, and fusion and growth of the hybrid protocells can be induced under conditions of high ionic strength. Our results highlight how notions of membrane-mediated compartmentalization, chemical enrichment and internalized structuration can be integrated in protocell models via simple chemical and physical processes.

The elucidation of plausible mechanisms of prebiotic compartmentalization offers important insights into how primitive processes of replication, metabolism and evolution could be embodied materially by spontaneous physical processes on the early Earth[1–3]. Among several scenarios, the self-assembly of fatty-acid vesicles has emerged as a dominant paradigm in the origin of life[4,5], and corresponding protocell models[6] have established that archetypal properties, such as small-molecule diffusion[7], macromolecular encapsulation and retention[8], spatially confined catalysis and replication[9,10], membrane-mediated pH gradients[11] and competitive growth and division[12,13], can be associated with these simple self-assembled systems. Although these observations provide strong support for the protocell vesicle hypothesis, the model fails to account for the high encapsulation efficiencies required to produce appropriate representations of the molecularly crowded, chemically enriched, structured milieu that is a hallmark of cellular organization[14]. In contrast, over 50 years ago Oparin suggested that the spontaneous phase separation and chemical enrichment in water of counter-charged polyelectrolytes into liquid microdroplets (coacervates) could provide a mechanism of prebiotic compartmentalization that is facile and independent of membrane (vesicle) formation[15].

Although numerous examples of biomolecular coacervation are known in synthetic systems[16–18], protocell models based on liquid microdroplet assembly have not advanced significantly since Oparin's initial experiments. However, a recent report demonstrated that coacervate microdroplets with a range of biomimetic functions could be assembled spontaneously from aqueous mixtures of biologically relevant peptides and mononucleotides of low molecular weight[19]. The peptide/nucleotide microcompartments are stable between pH values of 2 and 10 and up to temperatures of 85 °C, undergo pH-induced cycles of growth and decay, and comprise molecularly crowded aqueous interiors that are enriched in biomolecular components and display enhanced catalytic transformations. Significantly, the dielectric constant associated with the interior of the peptide/nucleotide droplets is lower than that of the surrounding continuous water phase, and as a consequence the microcompartments exhibit selective molecular sequestration, even though they are membrane free[19,20].

The above studies, along with recent reports on liquid–liquid phase separation in living cells[21,22], biomolecular partitioning and gene expression in cell lysate coacervates[23], ribonucleic acid (RNA) catalysis in molecularly crowded aqueous two-phase polymer systems[24] and multienzyme iterative processing in polymer/nucleotide coacervate microdroplets[25], suggest that it is timely to reconsider coacervate-mediated spatial compartmentalization and chemical enrichment as an alternative model of protocell organization. However, although the simplicity of coacervate assembly is attractive, the absence of an enclosing membrane is a major drawback of the model compared with vesicle-based approaches to microcompartmentalization.

To address this concern, here we develop a hybrid protocell model based on the spontaneous self-assembly of a fatty-acid membrane at the surface of preformed coacervate microdroplets. We test the generality of our approach using binary combinations of short- or long-chain cationic peptides (oligolysine, polylysine) or a synthetic polyelectrolyte (polydiallydimethylammonium chloride (PDDA)) with a negatively charged monoribonucleotide (adenosine triphosphate (ATP)) or a mixture of oligo- and polyribonucleotides. We show that the addition of sodium oleate at concentrations below the critical vesicle concentration results in the formation of membrane-bounded coacervate microdroplets that we propose as the basis for a new type of protocell model. In particular, the membrane-delineated microcompartments exhibit marked changes,

[1]Centre for Protolife Research and Centre for Organized Matter Chemistry, School of Chemistry, University of Bristol, Bristol BS8 1TS, UK, [2]Chemistry Department, Imperial College London, Exhibition Road, London SW7 2AZ, UK. *e-mail: s.mann@bristol.ac.uk

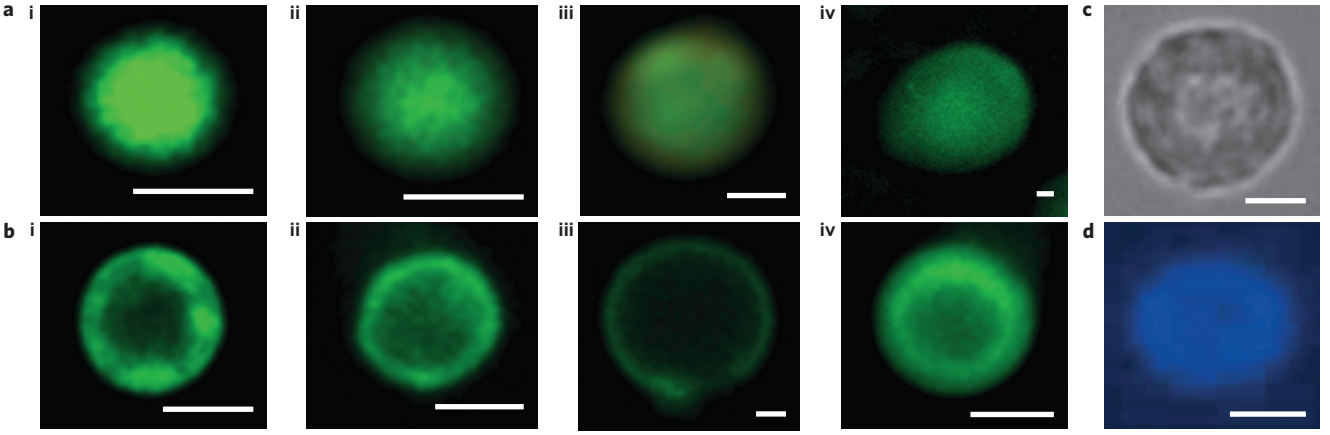

Figure 1 | Fatty-acid membrane self-assembly on the surface of positively charged coacervate microdroplets. Fluorescence microscopy images of single droplets stained with the lipid-soluble BODIPY FL C_{16} dye. **a**, Non-coated microdroplets showing homogeneous fluorescence throughout the interior of the microcompartments: **i**, polylysine/RNA (monomer molar ratio 1:0.5); **ii**, oligolysine/RNA (monomer molar ratio 1:0.25); **iii**, oligolysine/ATP (monomer molar ratio 1:0.17); **iv**, PDDA/ATP (monomer molar ratio 1:0.25). Scale bars, 1 μm. **b**, Oleate-coated droplets prepared from oleate/polylysine/RNA (pH 9, final molar ratio 0.67:1:0.5) (**i**), oleate/oligolysine/RNA (pH 9.3, 0.67:1:0.25) (**ii**), oleate/oligolysine/ATP (pH 8.7, 0.8:1:0.17) (**iii**) and oleate/PDDA/ATP (pH 10, 0.8:1:0.25) (**iv**) showing assembly of a fatty-acid membrane specifically at the surface of the microcompartments. Scale bars, 1 μm. **c**,**d**, Oleate/PDDA/ATP microdroplets prepared at a monomer molar ratio of 1.6:1:0.25 and doped with 0.1 mol% TNP-ATP: bright-field image of a single droplet (**c**) and the corresponding fluorescence microscopy image (**d**), which showing blue fluorescence from the TNP-ATP nucleotide in the fatty-acid-encapsulated coacervate matrix. Scale bars, 2 μm.

compared with uncoated coacervate droplets, in their ability to sequester or exclude various solutes from the external medium, such that concentration gradients can be established across the surface of the hybrid protocells. The coacervate-supported membrane is multilamellar, has a viscosity comparable to that of free-floating oleate/oleic acid vesicles and assembles specifically on the droplet surface under conditions not conducive to vesicle formation. Also, we demonstrate that the coacervate interior can be disassembled without loss of membrane integrity, and that fusion and growth of the hybrid protocells is induced under conditions of high ionic strength. Taken together, our results indicate that fatty-acid self-assembly and peptide/nucleotide coacervate formation can be assimilated into a novel protocell model that integrates notions of membrane-mediated compartmentalization, chemical enrichment and internalized structuration via the combination of simple chemical and physical processes.

Results and discussion

Hybrid protocell construction and molecular uptake/exclusion properties. Positively charged coacervate microdroplets were prepared at room temperature and neutral pH by the direct mixing of aqueous solutions of oligolysine ($M_w = 0.5$–2 kDa), polylysine ($M_w = 15$–30 kDa) or PDDA ($M_w = 150$ kDa) in combination with a mixture of oligo- and polyribonucleotides (torula yeast RNA, $M_w = 3$–80 kDa) or monomeric ATP under non-stoichiometric conditions (see Supplementary Methods). Coacervates were produced routinely at the following approximate monomer molar ratios (charge ratios): polylysine/RNA, 1:0.5; oligolysine/RNA, 1:0.25; oligolysine/ATP, 1:0.17 and PDDA/ATP, 1:0.25. In each case, stable dispersions of liquid microdroplets with diameters of a few to several tens of micrometres were observed by optical microscopy. Zeta potential measurements on the different types of coacervate droplets gave values in the range +4 to +30 mV (Supplementary Fig. 1). Assembly of a fatty-acid membrane on the surface of preformed polylysine/RNA, oligolysine/RNA or oligolysine/ATP microdroplets was undertaken at pH 8.5–9.3 by the single-step addition of aqueous sodium oleate at concentrations below the critical micelle concentration (CMC, ~3 mM). A similar method was also used to prepare oleate-coated PDDA/ATP microcompartments, although generally a two-step protocol was preferred at pH values above or equal to ten. In all cases, the addition of oleate monomers resulted in charge reversal to produce fatty-acid-coated microdroplets with negative surface potentials (Supplementary Fig. 1).

Fluorescence microscopy was used to confirm the presence of a fatty-acid membrane on the surface of each of the different types of coacervate microdroplets (see Supplementary Methods). For this, we employed a lipid-soluble boron-dipyrrin dye tagged with a 16-carbon chain (BODIPY FL C_{16} (Supplementary Fig. 2)) as a fluorescent probe for bilayer formation[26–28]. In the absence of oleate, the dye was readily sequestered into the coacervate phase to produce microdroplets that exhibited green fluorescence throughout their interior (Fig. 1a). As the solubility of the dye in water was very low, we attributed the preferential uptake to the reduced dielectric constant (ε) of the coacervate microdroplet interior ($\varepsilon \approx 55$) compared with that of the surrounding aqueous phase ($\varepsilon \approx 80$)[19]. In contrast, BODIPY FL C_{16}-stained images of oleate-containing coacervate droplets at monomer molar ratios of 0.67:1:0.5 (oleate/polylysine/RNA), 0.67:1:0.25 (oleate/oligolysine/RNA), 0.8:1:0.17 (oleate/oligolysine/ATP) and 0.8:1:0.25 (oleate/PDDA/ATP) indicated that the dye was located specifically on the surface of the microcompartments (Fig. 1b). To confirm the presence of an encapsulated coacervate phase, we prepared oleate/PDDA/ATP microdroplets at a molar ratio of 1.6:1:0.25 that were doped with a blue fluorescently tagged ATP derivative (2′,3′-*O*-(2,4,6-trinitrophenyl)adenosine-5′-triphosphate (TNP-ATP)). Fluorescence optical microscopy images showed blue fluorescence throughout the oleate-coated droplets (Fig. 1c,d).

Dynamic light scattering (DLS) experiments performed on oleate-coated PDDA/ATP microdroplets prepared at pH 10 showed a major peak at a mean hydrodynamic diameter (D_H) of 2 μm (Fig. 2a). Also, a peak at $D_H = 2$ μm was observed for the uncoated microdroplets (Fig. 2a), which indicates no significant change in the diameter of the microdroplets on the addition of oleate. This suggests that a continuous ultrathin fatty-acid shell, rather than, for example, an ensemble of discrete fatty-acid vesicles, surrounds the PDDA/ATP droplets. Importantly, as expected at pH 10, there was no evidence for a significant population of oleate micelles or vesicles in the coacervate dispersion (Fig. 2a). Similar observations were made for oleate-coated polylysine/RNA,

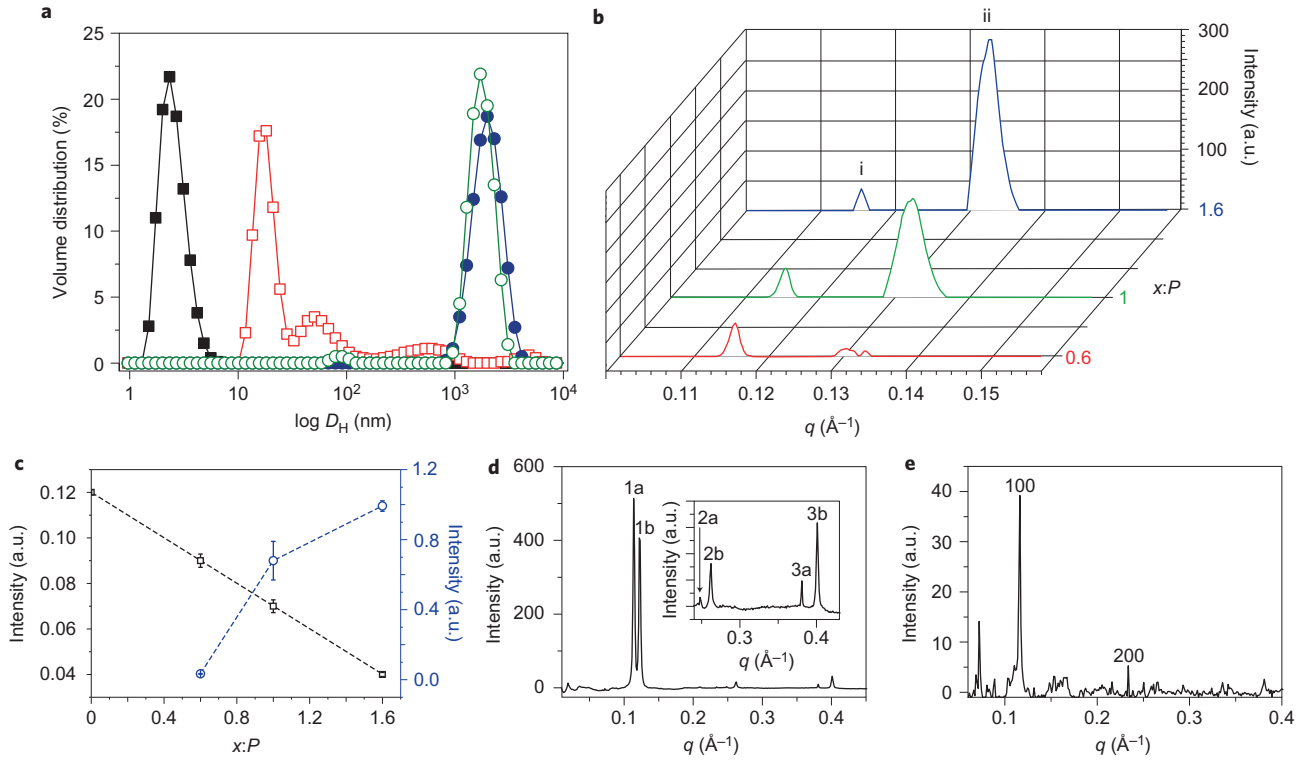

Figure 2 | DLS and SAXS measurements on coacervate droplets coated with fatty-acid membranes. a, DLS profiles showing volume distributions of hydrodynamic diameters (D_H (nm)) for oleate micelles (black filled squares, 20 mM oleate, pH 11), oleic acid/oleate multilamellar vesicles (red open squares, 20 mM, pH 8), uncoated PDDA/ATP microdroplets (blue filled circles, PDDA/ATP molar ratio 1:0.25 (*P*), pH 10) and oleate-coated PDDA/ATP microdroplets (green open circles, 1.6:*P*, pH 10.4). **b**, SAXS profiles of oleate/PDDA/ATP microdroplets prepared at 0.6:*P*, 1.0:*P* or 1.6:*P* at pH 10 showing non-related Bragg reflections at 5.46 nm (peak i) and 4.77 nm (peak ii) and their dependence on increasing oleate concentration (increasing *x*:*P*). **c**, Plot showing the changes in scattering peak intensity with increasing oleate concentration (increasing *x*:*P*) for the 5.46 nm (black open squares, left axis) and 4.77 nm (blue open circles, right axis) Bragg reflections shown in **b**; error bars relate to the deviation of the peaks from a Gaussian distribution. **d**, SAXS profile of a concentrated dispersion of oleate/PDDA/ATP microdroplets (1.6:1:0.25, pH 10.5) showing Bragg reflections that correspond to two multilamellar phases with interlayer spacings of $d_a = 5.51$ and $d_b = 5.06$ nm (peaks 1a, 2a, 3a and 1b, 2b, 3b, respectively). **e**, SAXS profile for oleic acid/oleate vesicles prepared at pH 8 showing a multilamellar phase with an interlayer spacing of 5.5 nm. a.u., arbitrary units.

oligolysine/RNA and oligolysine/ATP microdroplets (Supplementary Figs 3 and 4).

Synchrotron-radiation small-angle X-ray scattering (SAXS) was used to obtain structural information on the membrane associated with the oleate/PDDA/ATP coacervate droplets prepared over a range of oleate concentrations at pH 10. Previous SAXS studies on the uncoated PDDA/ATP coacervate phase showed no evidence for long-range mesostructural order[29]. In contrast, SAXS profiles from dispersions of the oleate/PDDA/ATP microdroplets at oleate concentrations at and above a monomer molar ratio of 0.6:1:0.25 showed two Bragg reflection peaks, which include a sharp reflection at 5.46 nm and a broad reflection at 4.77 nm (Fig. 2b). The latter reflection could be deconvoluted into two or three peaks with closely related *d* spacings depending on the oleate/PDDA/ATP molar ratio (Supplementary Fig. 5). Similarly, SAXS investigations of oleate/oligolysine/ATP microdroplets prepared at a molar ratio of 0.8:1:0.25 also showed two Bragg diffraction peaks with a minor reflection at 5.42 and a major peak at 4.90 nm (Supplementary Fig. 6). Significantly, the SAXS profiles of the oleate/PDDA/ATP samples under excess water conditions showed a considerable increase in the intensity of the Bragg peak at 4.77 nm as the oleate concentration increased, but the reflection at 5.46 nm decreased slightly (Fig. 2b,c). SAXS profiles of oleate/PDDA/ATP microdroplets (1.6:1:0.25, pH 10) that had been concentrated by approximately 30% by volume indicated that the oleate membrane was multilamellar in structure (Fig. 2d). Six sharp, intense Bragg reflections were observed for the oleate-coated coacervate microdroplets, and were assigned to two multilamellar phases with peak position ratios of 1:2:3, corresponding to Miller indices of (100), (200) and (300), and repeat interlayer spacings, *d*, of 5.51 and 5.06 nm (Fig. 2d). SAXS profiles on control samples of oleic acid/oleate vesicles prepared at pH 8.5 showed a multilamellar structure with an interlayer spacing of about 5.5 nm (Fig. 2e) (see the caption of Supplementary Fig 5 for a detailed analysis of the SAXS data).

The above observations are consistent with the self-assembly of oleate multilayers on the surface of the preformed coacervate microdroplets. As a consequence, we expected the membrane-bounded microcompartments to exhibit marked changes, compared with uncoated microdroplets, in their propensity to uptake or exclude various solutes present in the external medium (see Supplementary Methods). We tested this by using confocal fluorescence microscopy to assess changes in the uptake of cationic, zwitterionic and anionic dyes, as well as cofactors such as β-nicotinamide adenine dinucleotide (NADH) (for molecular structures, see Supplementary Fig. 2), all of which readily partitioned into the interior of uncoated, positively charged coacervate microdroplets (Fig. 3). In contrast, in the presence of the negatively charged oleate membrane, anionic dyes, such as calcein or fluorescein, were excluded from the droplet interior, such that confocal microscopy images of single droplets showed negligible fluorescence (Fig. 3). Uptake of the NADH dianion was also reduced, although some sequestration appeared to take place, which suggests that the fatty-acid membrane restricted diffusion of the cofactor into the

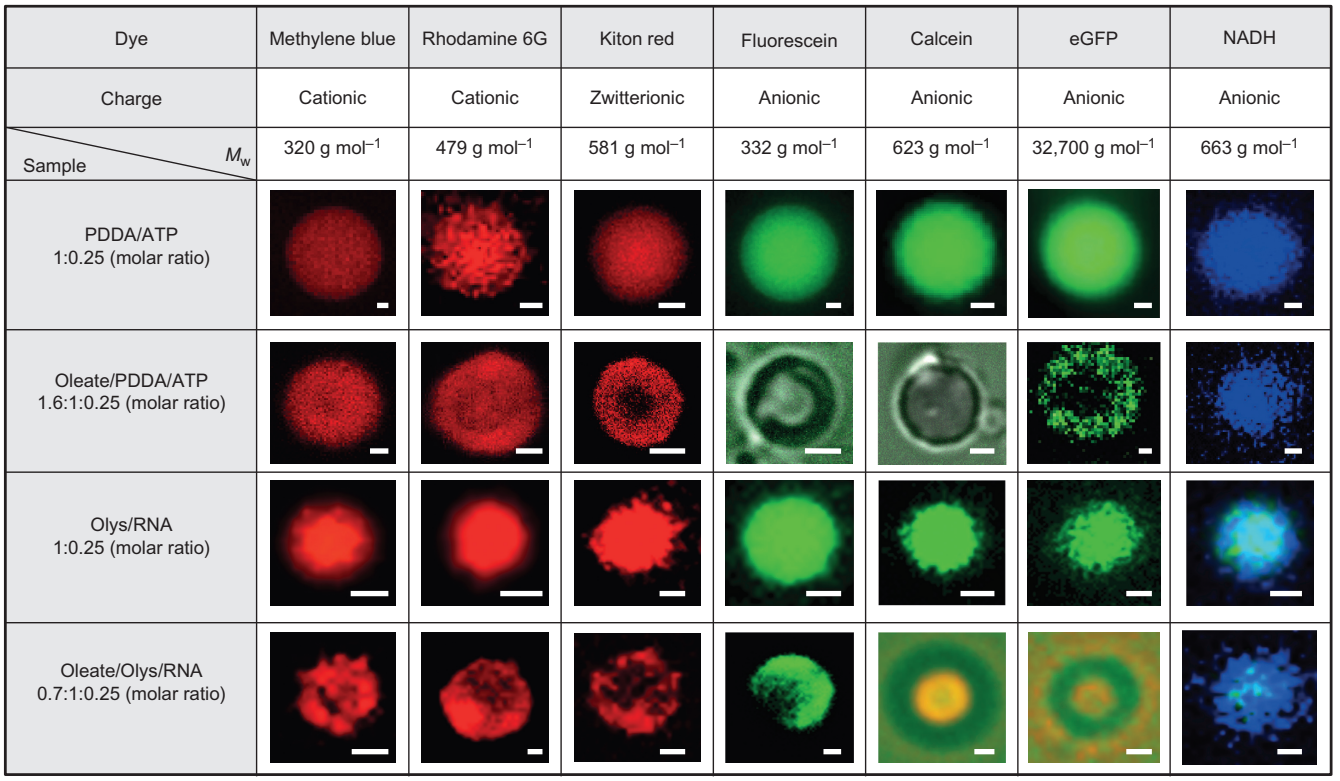

Figure 3 | Molecular uptake/exclusion from fatty-acid-coated PDDA/ATP and oligolysine/RNA coacervate microdroplets. Confocal fluorescence microscopy images that show uncoated or oleate-coated coacervate single droplets exposed to various cationic, anionic or zwitterionic solutes present in the external continuous aqueous phase. Images displayed in rows correspond to PDDA/ATP and oligolysine (Olys)/RNA coacervates and show homogeneous fluorescence throughout the droplets, which indicates that the chromophores are sequestered into the interior of the membrane-free protocells. In contrast, the images shown in the rows for oleate/PDDA/ATP and oleate/oligolysine/RNA display fluorescence only at the surface of the membrane-coated droplets (cationic dyes) or minimal fluorescence (anionic solutes), which indicates that the chromophores are excluded from the droplet interior. The exceptions are methylene blue and NADH, which are taken up into the membrane-coated droplets. Scale bars, 1 μm. eGFP, enhanced green fluorescent protein.

centre of the droplet. Positively charged dyes, such as rhodamine 6G and the zwitterionic molecule kiton red, were also excluded from the droplet interior and bound specifically at the membrane surface, although uptake of the cationic dye methylene blue, of lower molecular weight, was similar to that observed in the membrane-free microcompartments (Fig. 3). Taken together, the results were consistent with the presence of a semipermeable, negatively charged barrier at the surface of the oleate-coated coacervate microdroplets, and indicated that concentration gradients could be established across the assembled fatty acid membrane.

Coacervate-mediated fatty acid membrane assembly. Studies on the mechanism of fatty acid membrane assembly on the surface of the polyelectrolyte/ribonucleotide microcompartments were undertaken using positively charged PDDA/ATP microdroplets prepared by a two-step procedure at a PDDA monomer/ATP molar ratio of 1:0.25. In the first stage, an aqueous solution of sodium oleate micelles prepared at pH 11 was added to an aqueous dispersion of positively charged PDDA/ATP coacervate droplets (pH 10.5) to give a final pH of 10, oleate final concentration of 1.5 mM and oleate/PDDA/ATP monomer molar ratio of 0.32:1:0.25. Under these conditions, the total fatty-acid concentration was below the CMC (3.0 mM at pH 10, equivalent to a molar ratio of 0.7:1:0.25), such that anionic oleate monomers interacted with the positively charged polyelectrolyte/ribonucleotide droplets. In the second stage, a single aliquot of the sodium oleate micelles was added to the oleate/PDDA/ATP droplet dispersion to give monomer molar ratios that ranged from 0.4:1:0.25 to 2.4:1:0.25 at pH 10. Zeta potential measurements showed a progressive reduction in the positive surface charge of the droplets as the oleate concentration was increased in the coacervate dispersions (Fig. 4a). The droplets had an initial surface potential of +12 mV at a monomer molar ratio of 0:1:0.25, and became charge neutral at 0.6:1:0.25, below the CMC of the lipid. Higher levels of added oleate resulted in negative zeta potentials that became constant at a value of −60 mV at a molar ratio of 1.3:1:0.25. This value was similar to the potential recorded for oleate micelles alone at pH 11 (−65 mV). These observations were consistent with electrostatic binding of oleate monomers at the surface of the PDDA/ATP microdroplets, followed by assembly of multiple fatty-acid bilayers on the surface of the coacervate microcompartments at higher lipid concentrations.

We used fluorescence microscopy to image the PDDA/ATP microdroplets produced at various molar ratios of added oleate (Fig. 4b–e and Supplementary Fig. 7). Significantly, a homogeneous distribution of green fluorescence was observed throughout the droplets when BODIPY FL C_{16} was added to microcompartments treated with sub-CMC levels of oleate (oleate/PDDA/ATP monomer molar ratio of 0.32:1:0.25) (Fig. 4b). The images were analogous to those observed in the absence of oleate (see Fig. 1a), and indicated that the dye was able to access the droplet interior. Thus, binding of the oleate monomers to the positively charged droplets did not produce a continuous outer-membrane bilayer under these conditions. In contrast, charge-neutral or negatively charged oleate/PDDA/ATP droplets prepared between molar ratios of 0.4:1:0.25 and 1.6:1:0.25 showed a heterogeneous distribution of dye with increased fluorescence intensity specifically

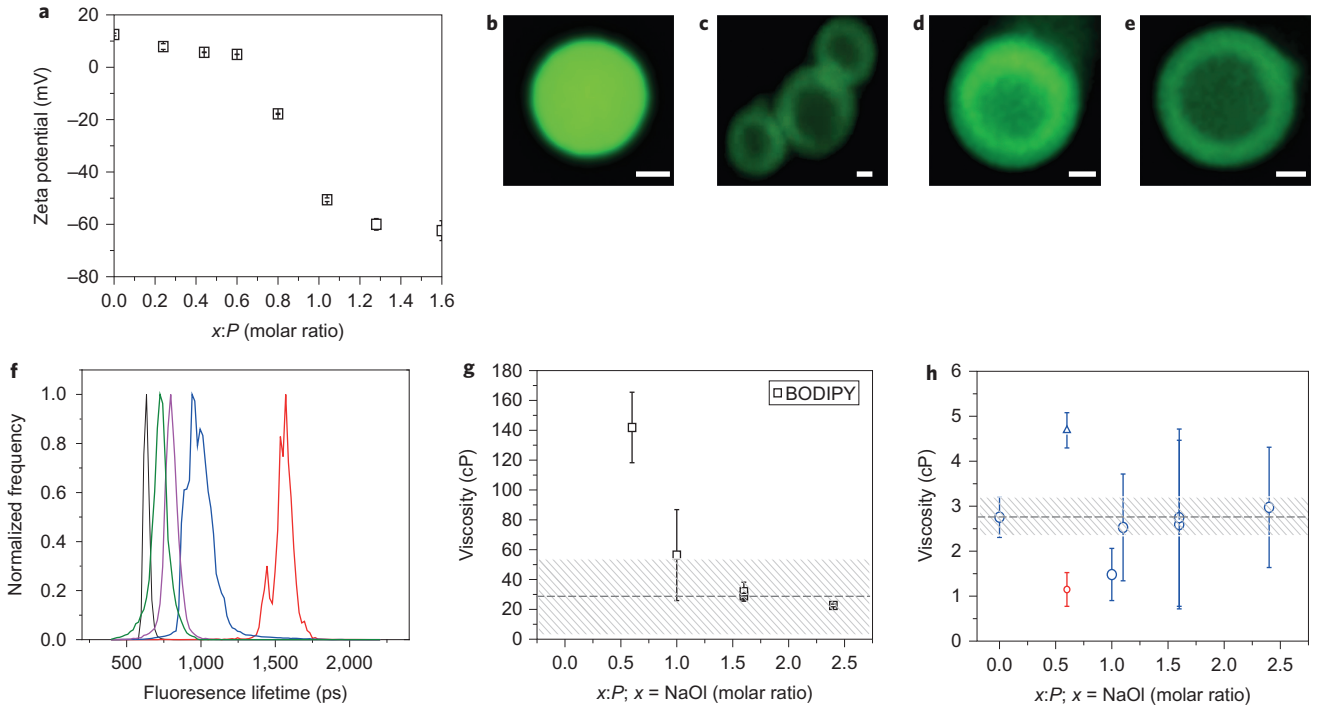

Figure 4 | Mechanism of coacervate-mediated membrane assembly. a, Plot of zeta potential for PDDA/ATP microdroplets prepared at various oleate concentrations (x): PDDA/ATP monomer molar ratios (x:P, where P = PDDA/ATP = 1:0.25). Lowering of the surface charge caused by electrostatic binding results in charge neutralization followed by charge reversal. **b–e** Fluorescence microscopy images of oleate-coated PDDA/ATP droplets stained with lipid-soluble BODIPY FL C_{16} dye at 0.32:P (**b**), 0.4:P (**c**), 1.0:P (**d**) and 1.6:P (**e**). Scale bars, 1 μm. Dye sequestration is present in **b** and membrane formation in **c–e**. **f**, Fluorescence lifetime distributions for membrane-solubilized BODIPY C_{10} in oleate-coated PDDA/ATP microdroplets prepared at pH 10 and molar ratios 0.6:P (red), 1:P (blue), 1.6:P (magenta) and 2.4:P (green). The control distribution for BODIPY C_{10} in oleic acid/oleate vesicles at pH 8 is shown in black. As the x:P ratio increases, the lifetime distributions narrow and the lifetimes approach that of the oleic acid/oleate vesicles. **g**, Plot of membrane viscosities derived from the fluorescence lifetime data shown in **f**; the dashed line and hatched area indicate the mean value and standard deviation, respectively, associated with the viscosity of the oleic acid/oleate vesicles at pH 8 (see Supplementary Fig. 11). The error bars mainly reflect the viscosity distribution in each image rather than low measurement accuracy. **h**, Plot of viscosity derived from the lifetime of Kiton red associated with the PDDA/ATP interior of uncoated (0:P) or oleate-coated microdroplets at various oleate (x):P molar ratios. Data points at 0.6:P (blue triangle and red circle) are anomalous because of charge-neutral conditions. The identical point in **g** also shows an anomalous oleate viscosity. Both data sets suggest instability of the microdroplets under these conditions. Error bars in **g** and **h** represent standard deviations.

on the surface of the microcompartments (Fig. 4c–e), consistent with the formation of a fatty-acid membrane. We attribute the formation of the membrane at pH values non-conducive to vesicle formation primarily to electrostatic interactions between the polyelectrolyte and oleate anions at the droplet surface, which reduces intermolecular repulsions between the negatively charged fatty-acid headgroups, which in turn lowers the monolayer interfacial curvature (see Supplementary Figs 8 and 9 for further mechanistic details).

Given these observations, fluorescence lifetime imaging microscopy (FLIM) was used to determine the changes in local viscosities (η) associated with the assembly of the fatty-acid membrane as well as the encapsulated PDDA/ATP coacervate matrix under different x:1:0.25 molar ratios (see Supplementary Methods). The PDDA/ATP matrix was probed using a coacervate-soluble molecular rotor (kiton red)[30], which was sequestered into the positively charged microdroplets prior to the addition of oleate. Alternatively, oleate-coated droplets were prepared without kiton red and the lipid layer was stained with BODIPY C_{10}, which served as a suitable molecular rotor for determining the viscosity of the fatty-acid membrane[30–32]. Significantly, the viscosity derived from the fluorescence lifetime of BODIPY C_{10} in the oleate surface layer of the droplets decreased progressively as the amount of added oleate was increased until it reached a value of 20–40 cP (1 cP = 1 mPa s), similar to that determined for a control sample of oleate/oleic acid vesicles (η = 20–40 cP) (Fig. 4f,g). In contrast, the local viscosity of the PDDA/ATP matrix associated with the microdroplets coated with fatty acid was much lower (1–4 cP), and was not significantly influenced by the amount of added oleate (Fig. 4h). The values were similar to those determined for the coacervate matrix of uncoated droplets (2.8 ± 0.4 cP, $\eta(H_2O) \approx 1$ cP), which indicated that encapsulation of the microdroplets by the lipid membrane did not significantly influence the local structure of the phase-separated compartment. In comparison, values for the membrane and coacervate viscosities determined at the onset of membrane assembly and close to charge neutrality (0.6:1:0.25) displayed anomalously high lifetimes for BODIPY C_{10} (1,680 ps ≈ 140 cP), and two distinct viscosity domains for kiton red (a short lifetime (<1 cP) at the droplet centre) and a longer lifetime (>4.5 cP) at the edge of the microcompartment (Fig. 4h). We attributed this to perturbations associated with the interaction of oleate with the coacervate matrix under charge-neutral conditions (Supplementary Fig. 10).

Hybrid protocell disassembly and growth. Internalized disassembly of the fatty-acid-coated polyelectrolyte/ribonucleotide droplets with retention of the oleate membrane was achieved by dispersing the hybrid protocells in aqueous solutions of high ionic strength (typically 75 mM). This was evidenced by FLIM experiments undertaken on oleate-coated PDDA/ATP microdroplets prepared at pH 10 at an oleate/PDDA/ATP monomer molar ratio of 1.6:1:0.25 and stained with either

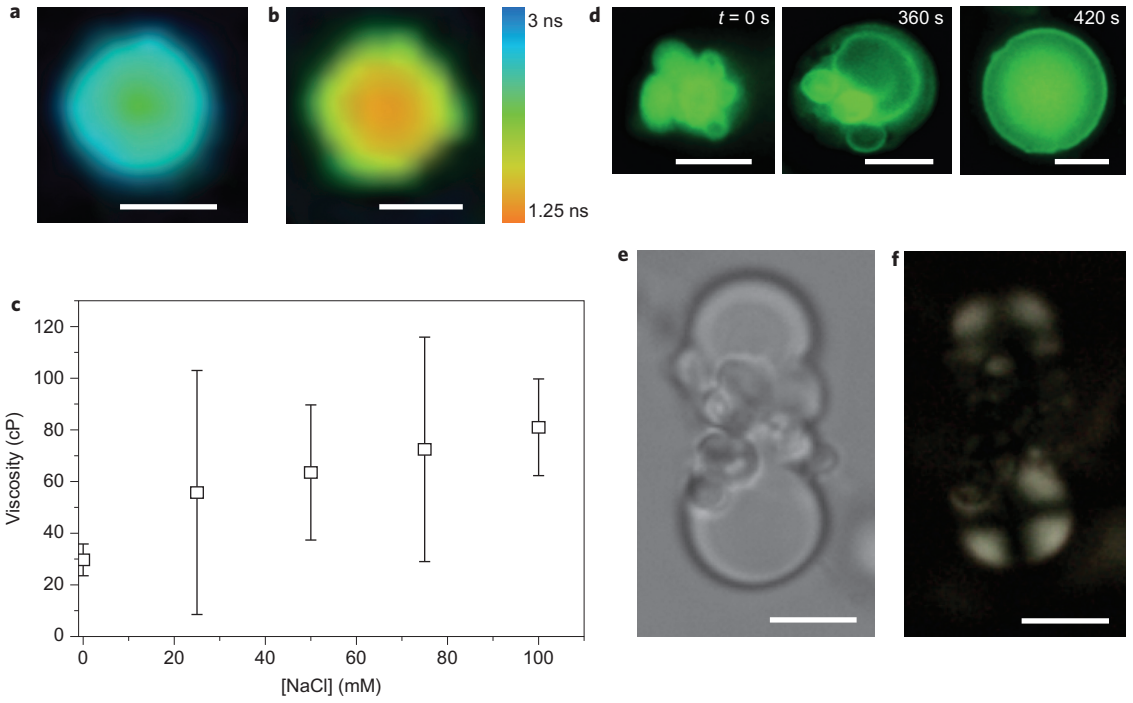

Figure 5 | Ionic-strength-induced coacervate disassembly and oleate membrane fusion in hybrid protocells. a,**b**, Fluorescence lifetime maps for oleate/PDDA/ATP microdroplets (monomer molar ratio 1.6:1:0.25) that contain kiton red in the absence (**a**) or presence (**b**) of 75 mM NaCl. The images show a marked reduction in the fluorescence lifetimes as a result of a reduction in the viscosity of the compartmentalized medium associated with the salt-induced disassembly of the membrane-enclosed coacervate. Scale bars, 5 μm. **c**, Plot of membrane viscosity derived from fluorescence lifetime maps as a function of NaCl concentration; error bars represent standard deviations. **d**, Time sequence that shows fluorescence images of BODIPY FL C_{16}-stained oleate/PDDA/ATP microdroplets (monomer molar ratio = 1.6:1:0.25) after the addition of 100 mM NaCl at $t = 0$, 360 and 420 s. Aggregation of the oleate-coated microdroplets occurs immediately after the addition of salt and results in fusion and growth of the microcompartments; the presence of the fluorescence dye throughout the fused microdroplets is indicative of the formation of densely packed multilamellar 'onion' vesicles. Scale bars, 5 μm. **e**,**f**, Bright-field (**e**) and cross-polarized (**f**) microscopy images of oleate/PDDA/ATP microdroplets in the presence of 100 mM NaCl. The maltese-cross textures characteristic of multilamellar 'onion' vesicles can be seen in **f**. Scale bars, 5 μm.

BODIPY C_{10}, or kiton red to measure the local viscosity of the fatty-acid membrane and polyelectrolyte/ribonucleotide interior, respectively, under varying salt concentrations ([NaCl] = 0 to 100 mM) that alone produced no changes in the fluorescence lifetime (control experiments). The results showed that increasing the salt concentration gave a decrease in the fluorescence lifetime of kiton red (Fig. 5a,b), which corresponded to a decrease in the viscosity of the encapsulated polyelectrolyte/ribonucleotide matrix from 2.7 ± 2.0 cP (no salt) to <1 cP, consistent with progressive disassembly of the PDDA/ATP coacervate phase. This was consistent with control experiments undertaken on uncoated droplets dispersed in highly ionic solutions (Supplementary Fig. 11). In contrast, the local viscosity of the fatty-acid membrane associated with the oleate-coated droplets increased in the presence of higher salt concentrations, which suggests that the bilayer structure was more compacted because of charge screening between the oleate headgroups (Fig. 5c). Control experiments on oleic acid/oleate vesicles were in agreement with these observations (Supplementary Fig. 11).

The above results indicated that disassembly of the coacervate droplet core could be accomplished at salt concentrations of 75 mM, without loss of the oleate multilayer membrane, to produce fatty-acid vesicles that contain a concentrated aqueous solution of encapsulated polyelectrolyte and ribonucleotide molecules. However, fluorescence microscopy images of BODIPY FL C_{16}-stained, fatty-acid-coated PDDA/ATP microdroplets (1.6:1:0.25) incubated with higher concentrations of salt (100 mM NaCl) at pH 10 indicated that under these conditions the microcompartments aggregated and fused to produce densely packed multilamellar 'onion' vesicles[33,34] (Fig. 5e,f), along with release of ATP to the external medium (Supplementary Fig. 12).

Conclusions

We used simple physical and chemical processes to demonstrate a new type of hybrid protocell model based on the spontaneous self-assembly of a continuous fatty-acid multilamellar membrane at the surface of preformed coacervate microdroplets that comprised molecularly crowded interiors. The approach integrates notions of membrane-mediated compartmentalization, chemical enrichment and internalized structuration, and brings together alternative models of prebiotic compartmentalization based on either phase-separated liquid droplets[15,19] or fatty-acid vesicle self-assembly[4,5,9,10]. Our studies indicate that the membrane-enclosed coacervate microcompartments are semipermeable and exhibit uptake and exclusion properties different to those of the uncoated microdroplets. Thus, it should be possible to exploit the hybrid protocell model to develop transmembrane control of coacervate-sequestered reaction systems such as gene-directed protein synthesis[23] or RNA catalysis[24] by diffusion-limited regulation of the uptake of small molecules from the external continuous aqueous phase.

Our studies include membrane-bounded coacervate droplets that are constructed from components of low molecular weight, such as cationic oligopeptides, ATP and oligoribonucleotides. Such molecules, along with fatty acids, can be considered as prebiotically relevant, which suggests that our hybrid protocell model is a plausible hypothesis for origin-of-life research that needs to be considered and developed further. For example, although fatty acid membrane assembly depends on the initial presence of preformed positively

charged coacervate microdroplets under the experimental conditions investigated, it seems feasible that less-stringent conditions might apply in the presence of highly heterogeneous mixtures of single-chain amphiphiles, monoribonucleotides and oligo-RNAs of low molecular weight. Indeed, compositional diversity is expected to be a hallmark of prebiotic environments, such that complex combinations of fatty acids with different chain lengths and headgroup chemistries, mononucleotides and nucleotide-derived cofactors (flavin adenine dinucleotide, NADH, etc.) with different nucleobase moieties and charge densities, and polyelectrolytes with variable polarity and solubility, could provide a diverse landscape of mechanisms for the spontaneous formation of membrane-delineated coacervate-based protocellular constructs. Although the development of combinatorial methods for exploring the design, construction, function and evolutionary potential of model protocells is in its infancy, such an approach should offer important insights into the mechanisms of prebiotic compartmentalization on the early Earth.

Received 1 October 2013; accepted 13 March 2014; published online 20 April 2014

References

1. Rasmussen, S., Chen, L. H., Nilsson, M. & Abe, S. Bridging nonliving and living matter. *Artif. Life* **9,** 269–316 (2003).
2. Luisi, P. *The Emergence of Life* (Cambridge Univ. Press, 2006).
3. Mann, S. Systems of creation: the emergence of life from nonliving matter. *Acc. Chem. Res.* **45,** 2131–2141 (2012).
4. Deamer, D. W. & Barchfeld, G. L. Encapsulation of macromolecules by lipid vesicles under simulated prebiotic conditions. *J. Molecul. Evol.* **18,** 203–206 (1982).
5. Monnard, P. A. & Deamer, D. W. Membrane self-assembly processes: steps toward the first cellular life. *Anat. Record.* **268,** 196–207 (2002).
6. Dzieciol, A. J. & Mann, S. Designs for life: protocell models in the laboratory. *Chem. Soc. Rev.* **41,** 79–85 (2012).
7. Deamer, D. W. & Dworkin, J. P. Chemistry and physics of primitive membranes. *Top. Curr. Chem.* **259,** 1–27 (2005).
8. Apel, C. L., Deamer, D. W. & Mautner, M. N. Self-assembled vesicles of monocarboxylic acids and alcohols: conditions for stability and for the encapsulation of biopolymers. *Biochim. Biophys. Acta* **1559,** 1–9 (2002).
9. Oberholzer, T., Wick, R., Luisi, P. L. & Biebricher, C. K. Enzymatic RNA replication in self-reproducing vesicles: an approach to a minimal cell. *Biochem. Biophys. Res. Commun.* **207,** 250–257 (1995).
10. Mansy, S. S. *et al.* Template-directed synthesis of a genetic polymer in a model protocell. *Nature* **454,** 122–125 (2008).
11. Chen, I. A. & Szostak, J. W. Membrane growth can generate a transmembrane pH gradient in fatty acid vesicles. *Proc. Natl Acad. Sci. USA* **101,** 7965–7970 (2004).
12. Zhu, T. F., Adamala, K., Zhang, N. & Szostak, J. W. Photochemically driven redox chemistry induces protocell membrane pearling and division. *Proc. Natl Acad. Sci. USA* **109,** 9828–9832(2012).
13. Adamala, K. & Szostak, J. W., Competition between model protocells driven by an encapsulated catalyst. *Nature Chem.* **5,** 495–501 (2013).
14. Fulton, A. B., How crowded is the cytoplasm? *Cell* **30,** 345–347 (1982).
15. Oparin, A. I. (1953) *The Origin of Life* 2nd edn (Dover Publications, 1953).
16. Evreinova, T. N., Karnaukhov, W. N., Mamontova, T. W. & Ivanizki, G. R. The interaction of biological molecules in coacervate systems. *Colloid Interface Sci.* **36,** 18–23 (1971).
17. de Kruif, C. G., Weinbreck, F. & de Vries, R. Complex coacervation of proteins and anionic polysaccharides. *Curr. Opin. Colloid Interface Sci.* **9,** 340–349 (2004).
18. Antonov, M., Mazzawi, M. & Dubin, P. L. Entering and exiting the protein–polyelectrolyte coacervate phase via non-monotonic salt dependence of critical conditions. *Biomacromolecules* **11,** 51–59 (2010).
19. Koga, S., Williams, D. S., Perriman, A. W. & Mann, S. Peptide–nucleotide microdroplets as a step towards a membrane-free protocell model. *Nature Chem.* **3,** 720–724 (2011).
20. Tang, T-Y. D., Antognozzi, M., Vicary, J. A., Perriman, A. W. & Mann, S. Small-molecule uptake in membrane-free peptide/nucleotide protocells. *Soft Matter* **9,** 7647–7656 (2013).
21. Brangwynne, C. P., Mitchison, T. J. & Hyman, A. A. Active liquid-like behavior of nucleoli determines their size and shape in *Xenopus laevis* oocytes. *Proc. Natl Acad. Sci. USA* **108,** 4334–4339 (2011).
22. Hyman, A. A. & Simons, K. Cell biology. Beyond oil and water—phase transitions in cells. *Science* **337,** 1047–1049 (2012).
23. Sokolova, E. *et al.* Enhanced transcription rates in membrane-free protocells formed by coacervation of cell lysate. *Proc. Natl Acad. Sci. USA* **110,** 11692–11697 (2013).
24. Strulson, C. A., Molden, R. C., Keating, C. D. & Bevilacqua, P. C. RNA catalysis through compartmentalization. *Nature Chem.* **4,** 941–946 (2012).
25. Crosby, J. *et al.* Stabilization and enhanced reactivity of actinorhodin polyketide synthase minimal complex in polymer/nucleotide coacervate droplets. *Chem. Commun.* **48,** 11832–11834 (2012).
26. Johnson, I. D., Kang, H. C. & Haugland, R. P. Fluorescent membrane probes incorporating dipyrrometheneboron difluoride fluorophores. *Anal. Biochem.* **198,** 228–37 (1991).
27. Kasurinen, J. A novel fluorescent fatty acid, 5-methyl-BDY-3-dodecanoic acid, is a potential probe in lipid transport studies by incorporating selectively to lipid classes of BHK cells. *Biochem. Biophys. Res. Commun.* **187,** 1594–601 (1992).
28. Rogers, R. A., Jack, R. M. & Furlong, S. T. Lipid and membrane protein transfer from human neutrophils to schistosomes is mediated by ligand binding. *J. Cell. Sci.* **106,** 485–91 (1993).
29. Williams, D. S. *et al.* Polymer/nucleotide droplets as bio-inspired functional micro-compartments. *Soft Matter* **8,** 6004–6014 (2012).
30. Hosny, N. A. *et al.* Fluorescent lifetime imaging of atmospheric aerosols: a direct probe of aerosol viscosity. *Faraday Discuss.* **165,** 343–356 (2013).
31. Wu, Y. *et al.* Molecular rheometry: direct determination of viscosity in Lo and Ld lipid phases via fluorescence lifetime imaging. *Phys. Chem. Chem. Phys.* **15,** 14986–14993 (2013).
32. Hosny, N. A. *et al.* Mapping microbubble viscosity using fluorescence lifetime imaging of molecular rotors. *Proc. Natl Acad. Sci. USA* **110,** 9225–9230 (2013).
33. Panizza, A., Roux, D., Vuillaume, V., Lu, C-Y. D. & Cates, M. E. Viscoelasticity of the onion phase. *Langmuir* **12,** 249–252 (1996).
34. Pommella, A., Caserta, S. & Guido, S. Dynamic flow behaviour of surfactant vesicles under shear flow: role of a multillamellar microstructure. *Soft Matter* **9,** 7545–7552 (2013).

Acknowledgements

We thank the Engineering and Physical Sciences Research Council (EPSRC, UK) and European Research Council (Advanced Grant) for financial support. We thank the EPSRC for a Career Acceleration Fellowship (grant number EP/E038980/1) to M.K.K. and the Malaysian government for the award of a PhD studentship to C.R.C.H. We acknowledge the Wolfson Bioimaging Facility (A. Leard) for assistance with confocal microscopy, beamline I22 (N. Terrill and A. Smith) at Diamond Light Source, W. Briscoe for beamtime and R. Richardson and M. Thomas for assistance and use of software for X-ray analysis. We thank W. Briscoe and J. Eastoe for helpful discussions.

Author contributions

S.M., A.W.P., T-Y.D.T., M.K.K. and D.S.W. conceived the experiments; C.R.C.H., A.J.T. and T-Y.D.T. performed the experiments; T-Y.D.T., A.J.T. and C.R.C.H. undertook the data analysis; T-Y.D.T., A.J.T., C.R.C.H. and S.M. wrote the manuscript. C.R.C.H. and A.J.T. contributed equally to the work.

Additional information

Supplementary information is available in the online version of the paper. Reprints and permissions information is available online at www.nature.com/reprints. Correspondence and requests for materials should be addressed to S.M.

Competing financial interests

The authors declare no competing financial interests.